Structure of the $[Zn_{In}\text{-}V_P]$ defect complex in Zn-doped InP

C. W. M. Castleton* and S. Mirbt
Theory of Condensed Matter, Department of Physics, Uppsala University, Box 530, 751 21 Uppsala, Sweden
(Received 3 March 2003; published 8 August 2003)

We study the structure, formation energy, binding energy and transfer levels of the zinc-phosphorus vacancy complex $[Zn_{In}\text{-}V_P]$ in Zn-doped *p*-type InP, as a function of the charge, using plane-wave *ab initio* density functional theory local density approximation calculations in a 64-atom supercell. We find a binding energy of 0.39 eV for the complex, which is neutral in *p*-type material, the $0/-1$ transfer level lying 0.50 eV above the valence-band edge, all in agreement with recent positron annihilation experiments. Our results indicate that, while the formation of phosphorus vacancies (V_P^{+1}) may be involved in carrier compensation in heavily Zn-doped material, the formation of Zn-vacancy complexes is not. Regarding the structure, for charge states $Q=+6\rightarrow-4$ the Zn atom is in an sp^2-bonded *DX* position and electrons added (removed) go to (come from) the remaining dangling bonds on the triangle of In atoms. This reduces the effective vacancy volume monotonically as electrons are added to the complex, resolving a recent debate between contradicting experiments. The reduction occurs through a combination of increased In-In bonding and increased Zn-In electrostatic attraction. In addition, for certain charge states we find complex Jahn-Teller behavior in which up to three different structures (with the In triangle dimerized, antidimerized, or symmetric) are stable and close to degenerate. We are able to predict and successfully explain the structural behavior of this complex using a simple tight-binding model.

DOI: 10.1103/PhysRevB.68.085203 PACS number(s): 71.55.Eq, 61.72.Bb, 71.70.Ej, 71.15.Dx

I. INTRODUCTION

Zn-doped *p*-type InP is one of the most common materials in use within optoelectronics. The Zn sits substitutionally within the In sublattice (Zn_{In}) where it has a shallow acceptor level. A well-known limitation in the use of Zn as a *p* dopant in InP is saturation of the hole concentration in the mid-10^{18}-cm^{-3} range. Above this further increases in Zn concentration do not translate into increases in the hole concentration. There are several suspected causes[1] for this, in particular (a) increases in the concentration of interstitial zinc (Zn_i), (b) phase separation, and (c) the formation of other compensating defects, especially phosphorus vacancies[1] (V_P) and complexes of zinc with V_P. In this paper we will examine the properties of Zn-V_P complexes, using *ab initio* methods.

The formation of one such Zn-V_P complex has been studied in Zn-doped Czochralski-grown InP by several groups, most recently by Mahony *et al.*[1] and Slotte *et al.*[2] Mahony *et al.* studied positron trapping rates and lifetimes measured over 0–300 K before and after rapid thermal anneals performed at 400–800 K, while Slotte *et al.* focused on the effects of annealing times and annealing temperatures upon the positron lifetimes and Doppler shifts of the emitted photons, with measurement temperatures up to 600 K. The Doppler broadening, which is sensitive to the atoms surrounding the defect in which the positron is trapped, allowed them to confirm that the complex observed is indeed a Zn-V_P pair, with a binding energy anticipated[3] (prior to detailed measurements) on the order of $0.1\rightarrow0.4$ eV. Both groups identify two separate positron lifetimes corresponding to two different forms of the same complex: a shorter lifetime of about 260–280 ps indicating an effective vacancy volume similar[1,4] to that of the free V_P and a longer lifetime of around 330 ps corresponding to a larger effective vacancy volume. Both groups identify the two forms as different charge states of the complex, the most stable (in *p*-type material) being neutral, with a $0/-1$ transfer level lying near the bottom of the band gap, 0.2 ± 0.1 eV above the valence-band edge according to Slotte *et al.* They believe[2] that the neutral form has a volume larger than the free vacancy and that the complex shrinks to a volume similar to the free vacancy when excited into its -1 charge state. This assignment comes primarily from the dependence of the positron lifetime on Zn density and measurement temperature for temperatures in the range 300–600 K. In contrast, Mahony *et al.* identify the larger volume as corresponding to the -1 charge state and the smaller to the neutral, a conclusion based upon the much larger trapping rate they measure for the longer positron lifetime as measured in the temperature range 0–300 K. (Slotte *et al.* do not report details of trapping rates in their measurements.) Hence there is an open question from experiment regarding the effective vacancy volume in the neutral- and negative-charge states.

A number of theoretical studies of the free phosphorus vacancy have been performed[5–7] using density functional theory (DFT). The free vacancy has been shown[6,7] to be a strong Jahn-Teller defect, indeed, to be a ''negative-*U*'' center in which the neutral-charge state V_P^0 is thermodynamically unstable relative to the $+1$ and -1 states. Hence a direct change $V_P^{-1}\rightarrow V_P^{+1}$ occurs as a function of increasing electron chemical potential (Fermi level). This is due to strong lattice relaxation in the -1 charge state. The vacancy is surrounded by a tetrahedron of four In atoms, each with a (partially filled) inwardly pointing dangling bond. In the -1 charge state a pair of dimers is formed: two opposing sides of the tetrahedron are reduced in length relative to the remaining four. The energy gained by this overcomes the Coulomb repulsion between the additional electrons, allow-

ing two electrons to be transferred onto the vacancy simultaneously.

In this paper we present what is, to our knowledge, the first *ab initio*[19] theoretical study of the $[Zn_{In}\text{-}V_P]$ complex, which we propose to be that observed in positron annihilation experiments. We will first describe the method in Sec. II. We will then report detailed results for the geometry and vacancy volume of the complex, both for the ground-state structures and for various metastable structures in Sec. III, followed by a description of how these vary with changes in the charge state of the complex in Sec. IV. In Sec. V we will also propose a simple tight-binding model which is able to predict almost all of the structural properties which we find. Finally, in Sec. VI we will conclude, relating our results to those from position annihilation and the issue of Zn compensation.

II. CALCULATIONAL DETAILS

We use plane-wave *ab initio* DFT (Ref. 8) within the local density approximation (LDA) together with ultrasoft pseudopotentials.[9,10] Calculations are performed using the VASP code.[11] Before doing calculations involving defects we first optimize the lattice parameter subject to the LDA. We find a value of 5.827 Å, compared to 5.869 Å experimentally, giving us a band gap of 0.667 eV, compared to 1.344 eV in experiment.

For defect calculations we use a 64-atom simple cubic supercell and allow all atoms not located on the surface of the cell to relax. This restriction is included to truncate the (spurious) elastic interactions between adjacent supercells. No restrictions are placed upon the symmetry of the relaxations. When calculating total energies of supercells containing charged defects we also include a uniform neutralizing background charge. The key quantity is the formation energy of the defect, E_d, defined[12] as

$$E_d = E^T(\text{defect}^Q) - E^T(\text{bulk}) + \sum_i \mu_i n_i + Q(e_v + e_f), \tag{1}$$

where $E^T(\text{defect}^Q)$ and $E^T(\text{bulk})$ are the total energy of the InP supercell with and without the charge Q defect. Both are calculated with the same values of the plane-wave cutoff, **k**-point grid, etc. in order to make use of the cancellation of errors. The defect is formed by adding (removing) n_i atoms, each with chemical potential μ_i, and by adding $(-Q)$ electrons, whose chemical potential e_f is measured from the valence-band edge e_v. We then adjust the various calculational parameters to converge E_d. We find that it is sufficient to use pseudopotentials in which Zn *d* electrons are treated as valence electrons but In *d* electrons are left in the core. We find that a plane-wave cutoff energy of 200 eV is enough to converge E_d to $O(0.01\text{ eV})$. Real-space projection operators are used, with the cutoff again chosen to give errors below $O(0.01\text{ eV})$.

The **k**-point convergence is more interesting, since we find different convergence behavior for the electronic and structural contributions to the formation energy $E_d(K)$, where we use a $K\times K\times K$ Monkhorst-Pack[13] **k**-point grid. The error in the electronic contribution to $E_d(\mathrm{K})$ is very close to the error in the unrelaxed formation energy $E_d^{UR}(K)$, which we can estimate as

$$\Delta^{UR}(N-M) = E_d^{UR}(N) - E_d^{UR}(M). \tag{2}$$

[We shall use $\{N,M\}=\{2,4\}$ and $\{4,6\}$ to estimate the errors in $E_d^{UR}(2)$ and $E_d^{UR}(4)$, respectively.] We cannot, of course, calculate the structural contribution directly, so we first define the relaxation energy

$$\epsilon_R(K) = E_d^R(K) - E_d^{UR}(K), \tag{3}$$

where $E_d^R(K)$ is the relaxed formation energy. We then estimate the convergence of $\epsilon_R(K)$ using

$$\Delta^R(N-M) = \epsilon_R(N) - \epsilon_R(M). \tag{4}$$

In Table I we list values of $\Delta^{UR}(2\text{-}4)$, $\Delta^{UR}(4\text{-}6)$, and $\Delta^R(2\text{-}4)$ for a range of charge states of various different

TABLE I. Comparison of the **k**-point convergence of the electronic and structural contributions to the formation energy E_d. Convergence of the electronic contributions is given by the change $\Delta^{UR}(N-M)$ in the unrelaxed formation energy when increasing the **k**-point grid from $N\times N\times N$ to $M\times M\times M$. Convergence of the structural contributions is given by $\Delta^R(N-M)$, the equivalent change in relaxation energy $\epsilon_R(N)$. See main text for full definitions.

Defect	$\Delta^{UR}(2\text{-}4)$	$\Delta^{UR}(6\text{-}4)$	$\Delta^R(2\text{-}4)$
V_{In}^{-4}	0.0082		−0.0190
V_{In}^{0}	−0.0483	0.0093	0.0368
In_i^{0}	0.0252	0.0052	
In_i^{+1}	−0.0539		−0.0037
In_i^{+3}	0.0206	0.0058	
In_i^{+4}	−0.1038		0.0061
P_{In}^{+1}	−0.0360		0.0246
P_{In}^{+2}	0.0314		0.0259
V_P^{-2}	−0.0607	−0.0123	
V_P^{+2}	0.0840	0.0012	
Zn_{In}^{+1}	0.0375		0.0007
Zn_{In}^{0}	0.0807	−0.0011	−0.0025
Zn_{In}^{-1}	−0.0004	0.0000	−0.0005
Zn_P^{+2}	−0.0266		0.0095
Zn_i^{+2}	0.0117	0.0001	0.0040
Si_{In}^{0}	0.0091		0.0091
Si_{In}^{+1}	0.0048		−0.0038
Si_{In}^{+2}	0.0891		0.0046
Si_P^{-2}	0.0296		−0.0006
Si_P^{-1}	0.0031		0.0008
Si_P^{0}	0.0734		−0.0027
Si_P^{+1}	0.0279		0.0004
$[Zn_i\text{-}V_P]^{+3}$	0.0272		0.0151
$[Zn_{In}\text{-}V_P]^{-1}$	−0.0750		0.0046
$[Zn_{In}\text{-}V_P]^{0}$	0.0057		−0.0029
$[Zn_{In}\text{-}V_P]^{+1}$	−0.0598		0.0184

defects in InP. We find that when atomic relaxations are ignored, a $2\times2\times2$ **k**-point grid produces errors around $O(0.01\ \text{eV})$, provided $Q=0$ [column $\Delta^{UR}(2\text{-}4)$ of Table I]. When $Q\neq0$, however, we find that the error introduced by truncating at $2\times2\times2$ increases with $|Q|$. Instead, a $4\times4\times4$ grid is required: column $\Delta^{UR}(4\text{-}6)$ indicates that this is sufficiently converged. On the other hand, the relaxation energy $\epsilon_R(K)$ converges faster; see column $\Delta^{R}(2\text{-}4)$ in the table. Indeed, $\epsilon_R(K)$ is converged for a $2\times2\times2$ Monkhorst-Pack grid, for any value of Q. In other words the structural contribution to E_d appears to converge faster with the **k**-point grid than the electronic contributions. This is largely due to a double cancellation of errors when we calculate ϵ_R from values of E_d which already contain a cancellation of errors. It means that, although we should use a $4\times4\times4$ grid to obtain an accurate value for E_d^R, we can save much calculation time by estimating $E_d^R(4)$ as

$$E_d^R(4)\approx E_d^{UR}(4)+\epsilon_R(2)=E_d^{UR}(4)+E_d^R(2)-E_d^{UR}(2). \tag{5}$$

The resulting values of $E_d^R(4)$ are converged to at least 0.02–0.04 eV and usually to an order of magnitude or so better. Hence we do most relaxations with a $2\times2\times2$ **k**-point grid, only checking key ones at $4\times4\times4$. Charge and electron localization function[14] (ELF) plots are, on the other hand, calculated using a $4\times4\times4$ **k**-point grid at the $2\times2\times2$ related structures.

III. NEUTRAL $[Zn_{In}\text{-}V_P]$ COMPLEX

A. Formation and binding energies

In order to calculate absolute values for the formation and binding energies we need to know the chemical potentials μ_{In}, μ_P, and μ_{InP}. Fully converged calculations for In, P (black phosphorus), and InP (the latter in its basic two-atom fcc cell) give the bulk values[20] -3.270 eV, -6.028 eV, and -9.728 eV, respectively. For pure InP we have, at thermodynamic equilibrium, $\mu_{InP}=\mu_{In}+\mu_P$. In In-rich material we then have $\mu_{In}=-3.270$ eV, leading to $\mu_P=-6.459$ eV, while in P-rich material $\mu_P=-6.028$ eV and hence $\mu_{In}=-3.700$ eV. We now use the values $\mu_{In}=-3.485$ eV and $\mu_P=-6.243$ eV, corresponding to exactly stoichiometric conditions. Properly, doping with Zn should alter these μ values, but even a Zn concentration of $5\times10^{18}\ \text{cm}^{-3}$ only corresponds to replacing 1 In in 2000 with Zn. We thus ignore the effect and use the fully converged bulk value -1.891 eV for μ_{Zn}.

Since we are primarily interested in strongly *p*-type material, we assume that the electron chemical potential lies at the valence-band edge, meaning that $e_f=0$. Using fully relaxed calculations in the 64-atom simple cubic cell, we find that the most stable charge states of the Zn_{In} and V_P are -1 and $+1$, respectively, while for $[Zn_{In}\text{-}V_P]$ it is 0. The formation energies are $E_d(Zn_{In}^{-1})=0.32$ eV, $E_d(V_P^{+1})=1.96$ eV, and $E_d([Zn_{In}\text{-}V_P]^0)=1.89$ eV. For V_P we find a free vacancy volume of 7.2 Å^3, where we calculate only the volume of the tetrahedron formed by the four In surrounding the vacancy. V_P^{+1} is invisible to positrons, however, so the positron annihilation experiments detecting free V_P in semi-insulating[1] and *n*-type material[4] will correspond to V_P^0 (volume 5.9 Å^3) or V_P^{-1} (volume 4.7 Å^3). More detailed results about V_P and Zn_{In} will appear elsewhere.[15]

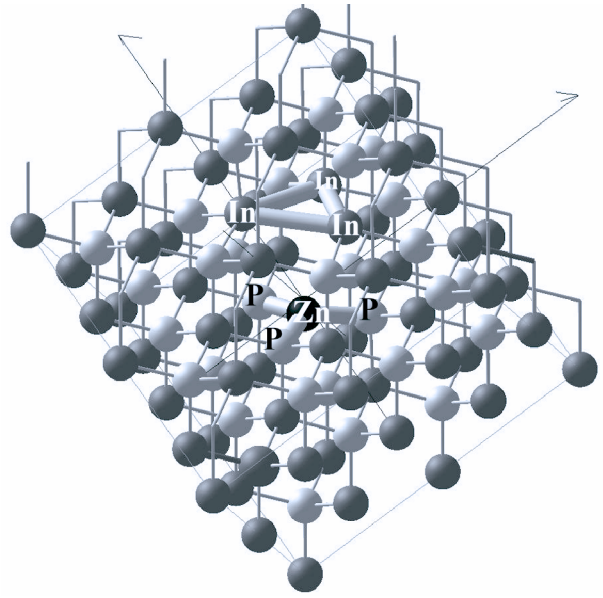

FIG. 1. Structure of the supercell containing the neutral $[Zn_{In}\text{-}V_P]$ complex. Atom types are dark gray, In; pale gray, P; black, Zn.

We can evaluate the binding energy E_b of the complex as

$$E_b([Zn_{In}-V_P]^0)=E_d(Zn_{In}^{-1})+E_d(V_P^{+1})-E_d([Zn_{In}-V_P]^0) \tag{6}$$

This gives us a value of 0.39 eV, which agrees with the 0.1 $\rightarrow$0.4 eV estimate from the positron annihilation experiments.[3]

B. Structure

In Fig. 1 we show the relaxed structure of the $[Zn_{In}\text{-}V_P]$ complex in the $Q=0$ charge state. The Zn_{In} is bonded to three P atoms only and has relaxed back into a *DX*-like position in the same plane as those P atoms. The resulting Zn-P distances are 2.31 Å, which is almost identical to the 2.34 Å value we find for the shorter Zn-P distances in a similar DFT-LDA calculation for Zn_3P_2 and various other Zn-P binary compounds.[16] The three In atoms on the other side of the V_P have moved together slightly, giving three equal In-In distances of 3.69 Å, compared to an ideal LDA bulk next-nearest-neighbor distance of 4.12 Å. The Zn-In distance is rather longer than the bulk value, however, at 4.41 Å. This gives a volume for the vacancy of 7.58 Å^3, where we calculate the volume of the tetrahedron formed by the three In and the Zn, in analogy to our volume estimation for free vacancies. This volume for the complex is thus rather larger than that for the neutral or negative free V_P. In the remaining figures most of the atoms in the cell are omitted for clarity, and lines are drawn around the edges of the tetrahedron to guide the eye. In the case of Zn-In lines they do *not* represent bonds. This can be seen clearly by examining the ELF (Ref.

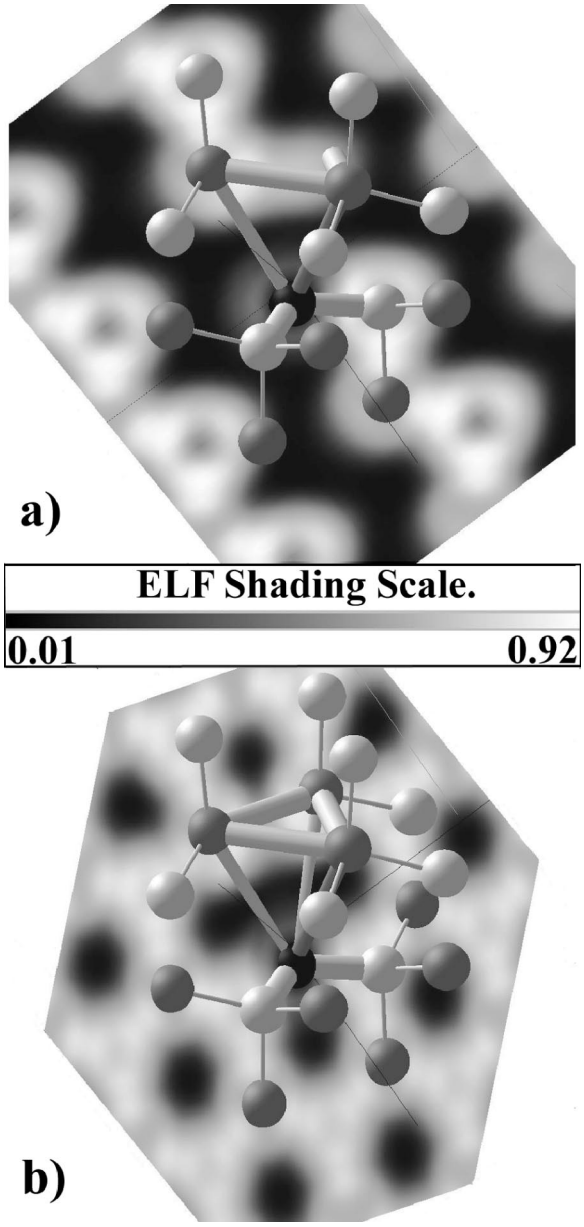

FIG. 2. (a) ELF plots for the neutral $[Zn_{In}\text{-}V_P]$ complex. For clarity most atoms are omitted and the edges of the Zn-In tetrahedron are drawn. Note, however, that there are *no* Zn-In bonds. (a) ELF in a plane containing Zn, 1 In, and the (111) axis. (b) ELF in a plane containing Zn and 2 In.

14) plots in Fig. 2. The ELF is the ratio of the kinetic energy density at a particular point in space to the kinetic energy density in a homogenous electron gas of the same charge density, normalized to take values from 0 to 1. Hence a value of ELF close to 1 indicates a region of increased kinetic energy density, corresponding to increased electron localization: roughly, a region of chemical bonding. Here, we see ELF values close to 0 in the region between the Zn and In triangle, indicating that there is no bonding between them. Instead, the Zn has three sp^2 hybrid orbitals bonded to the surrounding P, these bonds being filled. There is no density related to the Zn at all along the line perpendicular to the Zn-P plane [the (111) axis]. This suggests that the single Zn $4p_z$ orbital left over from the formation of the sp^2 hybrids is empty, a conclusion which will be confirmed in the following sections.

TABLE II. Transfer levels of $[Zn_{In}\text{-}V_P]$, in the 64-atom cell, relative to the valence-band edge.

Level	Energy
$+6/+5$	-0.51 eV
$+5/+4$	-0.51 eV
$+4/+3$	-0.47 eV
$+3/+2$	-0.44 eV
$+2/+1$	-0.37 eV
$+1/0$	-0.32 eV
$0/-1$	0.50 eV
$-1/-2$	0.70 eV
$-2/-3$	0.95 eV
$-3/-4$	1.05 eV
$-4/-5$	1.19 eV
$-5/-6$	1.18 eV

IV. STRUCTURE OF $[Zn_{In}\text{-}V_P]$ AS A FUNCTION OF CHARGE STATE

A. Bond lengths and vacancy volumes

In Table II we give the positions of a number of transfer levels of the complex, covering the charge states $+6 \rightarrow -6$. Several of these levels lie within the valance or conduction bands when evaluated within this supercell, but this may change in larger supercells (or with the LDA band-gap problem), so some may still be relevant to real materials. On the other hand, the structures of these states, listed in Table III, are likely to be more accurate than the energies and it is trends within these structures which we wish to examine in this paper. We note first that the structures of all of the states are actually very similar. For all $Q>-5$ the Zn lies in the *DX*-like position. The three In atoms remain unbonded to Zn, but both the In-In distances and the Zn-In distances shorten with increasing negative charge. This reduces the vacancy volume for each additional electron. Hence our calculations are in agreement with the conclusions of Slotte *et al.*, who found[2] that the effective volume was reduced when going from $Q=0$ to $Q=-1$, and in disagreement with those of Mahony *et al.*, who found[1] the opposite. The specific volume we find for $Q=-1$ (6.5 Å^3) is a little larger than the calculated free vacancy volumes of 5.9–4.7 Å^3 for the free vacancy but it is similar and the trend is certainly correct. The monotonic reduction in volume with number of electrons holds until $Q=-5$, when the Zn $4p_z$ orbital starts to be filled, leading at $Q=-6$ to a non-*DX* position for the Zn atom, with the Zn-In distance only 1.6% longer than the In-In. The transfer level into this state lies 1.18 eV above the valence-band edge. With the LDA band gap being only 0.67 eV this places the level about 0.51 eV above the conduction-band edge. This orbital also displays a negative *U* effect: the $Q=-5$ structure—which lies half way between *DX* and non-*DX* forms—is thermodynamically unstable, so the trans-

TABLE III. Geometry of the most stable form of $[Zn_{In}\text{-}V_P]^Q$ as a function of Q. Distances in Å, volumes in Å^3. Most structures (Str.) found are symmetric (SY) (all In-In distances equal, all Zn-In distances equal.) Where the In-In (and likewise Zn-In) distances differ it is found that two remain equal [In-In(2)] and one is different [In-In(1)] by amount Δ(In). [In-In(1)]<[In-In(2)] corresponds to the formation of a dimer (DM) and [In-In(1)]>[In−In(2)] to an antidimer (AD).

Q	Zn-P	Zn-In (1)	Zn-In (2)	In-In (1)	In-In (2)	Volume	Str.	Δ(In)
+6	2.29	4.97		4.95		14.36	SY	
+5	2.29	4.97		4.96		14.42	SY	
+4	2.29	4.98		4.97		14.49	SY	
+3	2.29	4.97		4.99		14.53	SY	
+2	2.29	4.99		4.97		14.57	SY	
+1	2.30	4.69		4.36		10.86	SY	
0	2.30	4.41		3.69		7.58	SY	
−1	2.30	4.23	4.31	3.64	3.37	6.52	AD	7.9%
−2	2.31	4.13	4.20	3.52	3.19	5.81	AD	10.3%
−3	2.32	3.95	4.10	2.99	3.28	5.23	DM	8.9%
−4	2.32	3.96		3.08		4.85	SY	
−5	2.43	3.21		3.04		3.59	SY	
−6	2.51	2.99		2.95		3.09	SY	

fer level $-5/-6$ lies just below the $-4/-5$ level. Hence we would anticipate instead a $-4/-6$ level about 0.5 eV above the conduction-band edge. However, conclusions about levels this deep into a band are, of course, rather unreliable since the wave functions should be very delocalized. The main point is that the Zn $4p_z$ level lies some way above the In-dangling-bond-based levels, confirming the conclusion that it is empty for $Q=+6\rightarrow-4$.

In addition to the general monotonic volume decrease, Jahn-Teller effects are apparent for $Q=-1\rightarrow-3$, in which one In-In distance is shortened (dimerized) or lengthened (antidimerized) relative to the other two. These remaining In-In distances always remain equal to at least 0.001 Å.

In Table IV we show the various metastable structures (structural excitations) which we find. (An extensive search suggests that there are no other metastable structures besides these.[21]) The fact that the Zn $4p_z$ level lies well inside the conduction band is further underlined by the metastable structures seen for $Q=-5$ and $Q=-6$. For both of these we find a *DX*-like metastable structure very similar to the ground-state structure of the $Q=-4$ state. This indicates that one or two electrons (respectively) have been transferred from the complex into the conduction band, leaving the complex with an empty Zn $4p_z$ and additional charge elsewhere in the supercell. The energy splitting between these *DX* and non-*DX* forms is therefore expected to change significantly (indeed, to switch over) in larger supercells where less defect level dispersion is seen. A similar effect is seen in the $Q=+1\rightarrow+4$ charge states, where a metastable structure is found which closely resembles the $Q=0$ structure. Since the hole levels corresponding to these charge states lie below the valence-band edge, these structural excitations amount to exciting holes off the complex, leaving it in the $Q=0$ charge state, with additional charge elsewhere. (An equivalent structural excitation for $Q=+5$ or $+6$ has not been found—presumably the excitation energy involved is too great for even metastability within this supercell.)

TABLE IV. Geometry of structural excitations of $[Zn_{In}\text{-}V_P]^Q$ as a function of Q. Energies are given relative to the energy of the most stable structures, as listed in Table III. See Table III also for the meaning of other columns and notation.

Q	Energy [eV]	Zn-P	Zn-In (1)	Zn-In (2)	In-In (1)	In-In (2)	Volume	Str.	Δ(In)
+4	1.00	2.30	4.44		3.74		7.85	SY	
+3	0.97	2.30	4.44		3.76		7.91	SY	
+2	0.93	2.30	4.44		3.72		7.76	SY	
+1	0.12	2.30	4.42		3.71		7.67	SY	
−1	0.011	2.30	4.29	4.27	3.41	3.50	6.57	DM	2.7%
−1	0.012	2.30	4.28		3.47		6.58	SY	
−2	0.03	2.31	4.18	4.17	3.22	3.35	5.85	DM	3.7%
−3	0.02	2.31	4.05	4.10	3.41	3.06	5.26	AD	11.6%
−3	0.05	2.31	4.08		3.18		5.31	SY	
−5	0.02	2.34	3.67		3.05		4.32	SY	
−6	0.19	2.34	3.63		3.05		4.26	SY	

All of the other excited structures found in the calculations relate to various Jahn-Teller distortions and affect only the In-In and Zn-In bond lengths. They involve no significant changes in vacancy volume, Zn position, or electron occupancy of the complex (see next subsection). The energies involved are very small indeed: on or below the order of room-temperature thermal energies. Room-temperature experiments are therefore likely to see averages over these structures. Three possible structures are found to be stable: one In-In bond dimerized (the other two equal), one antidimerized, or all equal. How the symmetric structure comes to be stable despite the Jahn-Teller effect will be returned to in Sec. V. All three structures are found to be stable for $Q=-1$ and $Q=-3$, but for $Q=-2$ the symmetric structure is not seen. For $Q=0$ and $+1$ we find only the symmetric structure.

The energy separations between these structures are beyond the limits of what we expect to resolve using only the $2\times2\times2$ Monkhorst-Pack **k**-point grid together with Eq. (5). As a result we have recalculated the energies and structures of all of these states using a $4\times4\times4$ **k**-point Monkhorst-Pack grid and, for some, even a $6\times6\times6$ grid. We find that all of the structures reported in Tables III and IV remain stable, although the degree of dimerization or antidimerization changes in some cases. The order of stability for the three structures changes for $Q=-1$ and $Q=-3$, however, and in all charge states they move closer to degeneracy. These changes are illustrated in Table V. The structural excitation energies are still smaller than the estimated accuracy levels of our formation energies. A further cancellation of errors does improve the accuracy (the excitation energies are differences of formation energies) but the separations remain so small that our prediction of the order of the excitations is not certain.

TABLE V. *Ab initio* results for the lowest-lying structures (marked L.L.) of $[Zn_{In}\text{-}V_P]^Q$ for $Q=+2\rightarrow-4$, together with structural excitation energies in electron volts. DM=dimerized, SY=symmetric, and AD=antidimerized. "-" indicates that the structure is not stable.

Q	DM	SY	AD
+2	-	L.L.	-
+1	-	L.L.	-
0	-	L.L.	-
−1	L.L.	0.0004	0.0001
−2	0.0002	-	L.L.
−3	0.0097	0.0104	L.L.
−4	-	L.L.	-

B. Charge density differences

In Fig. 3 we show the instantaneous change in charge density when an electron is added to (upper row) or removed from (lower row) the $Q=0$ charge state. In other words, we first take the $Q=0$ relaxed positions and calculate with the $Q=-1$ or $Q=+1$ total charge. We then subtract from this new charge density the original charge density from the relaxed $Q=0$ calculation. The isocharge surfaces plotted are for 80%, 50%, and 20% of the peak value. It is clear that an electron added goes to a localized orbital on or near the In triangle. An electron removed, however, comes from a delocalized state. We note, however, that even for the 20% peak value isocharge surface for $0/-1$, the total charge enclosed corresponds to only 0.48 electrons. Hence, even for the $Q=-1$ charge state, most of the added electron has an apparently delocalized character. This is, however, a result of the use of a relatively small supercell: the In-In distance is 3.7 Å *within* the cell, but about 9.2 Å between cells. This produces a significant fake dispersion for the defect levels and means that the transfer levels given in Table II should not be trusted too heavily.

In Fig. 4 we show the 50% peak isocharge surface for the instantaneous charge density change upon adding or removing electrons from the symmetric structures for $Q=+1$, 0, and -1. The orbital filled when adding an electron to $Q=0$ and that emptied when removing an electron from $Q=-1$ are essentially the same. Clearly $Q=-1$ is a localized state of the $[Zn_{In}\text{-}V_P]$ complex. Adding an electron to the $Q=-1$ state gives a very similar shaped charge density—the opposite spin state of the same orbital.

Removing an electron from $Q=0$ empties a delocalized valence-band state, as can be anticipated from the transfer level being found inside the valence band in the previous section. However, adding an electron to the (fully relaxed) $Q=+1$ fills an In triangle localized orbital, nonetheless. Clearly $Q=+1$ also corresponds to a localized state of the complex.

Going beyond $+1$ and -1, Fig. 4 also indicates a pattern which we in fact find for all charge states from $+6$ to -6: the electrons added or removed at the transfer levels $+2/+1$ and $+1/0$ come from essentially the same orbital, which we shall call Φ_0. The same is also true for the orbitals corresponding to other transfer level pairs: $0/-1$ and $-1/-2$, (labeled Φ_1), $-2/-3$ and $-3/-4$ (labeled Φ_2), and $-4/-5$ and $-5/-6$ (labeled Φ_3). Rather than plot all of them we show only one example of each orbital (transfer level pair). For the first three of these orbitals the shape is best seen in a top view, looking down the (111) axis. This is shown in Fig. 5 for the symmetric, dimerized, and antidimerized structures. A clear relationship emerges: the dimer orbital for $0/-1$ is very similar to the antidimer orbital for $-2/-3$. Likewise, the dimer orbital for $-2/-3$ and the antidimer orbital for $0/-1$ are the same. Furthermore, a symmetric combination (addition) of these two would give an orbital very much like that of the symmetric $-2/-3$ orbital. An antisymmetric combination (subtraction) would give something similar to the symmetric orbital for $0/-1$, although in this case the similarity is not complete. This may

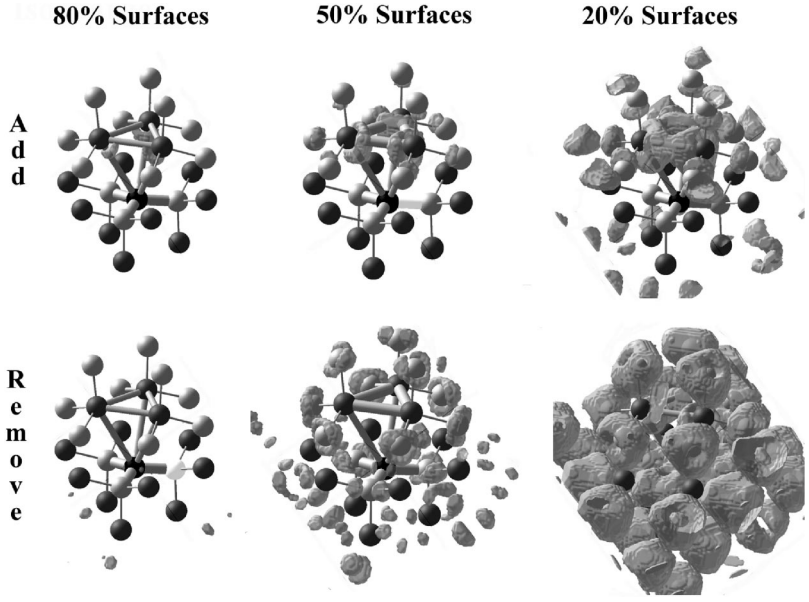

FIG. 3. Charge density difference plots for the $[Zn_{In}\text{-}V_P]$ complex in the $Q=0$ relaxed geometry, but with an extra electron added (upper row) or removed (lower row). Shown are isocharge surfaces for the charge density difference itself. The surfaces shown are for 80%, 50%, and 20% of the peak value.

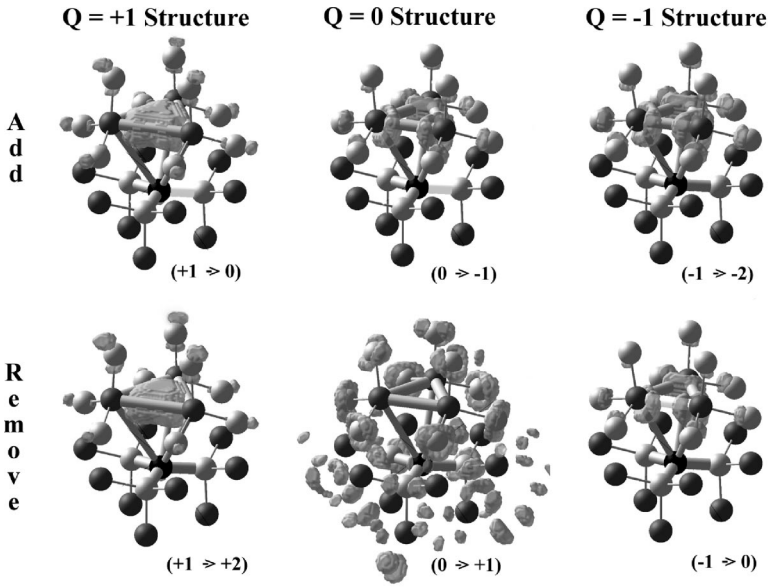

FIG. 4. 50% isosurface plots for charge density differences for adding (top row) and removing (bottom row) electrons from the $Q=+1$, 0, and -1 relaxed structures for [Zn_{In}-V_P].

be due to differences in the degrees of dimerization or perhaps to limitations in the calculation. Despite this, a clear relationship between the orbitals filled or emptied at these transfer levels in the three nearly degenerate structures is present and will be considered in more detail in Sec. V.

For the orbital Φ_3 (associated with $-4/-5$ and $-5/-6$) we show a side view in Fig. 6. It is the Zn $4p_z$ orbital, as expected based upon the structures reported in the previous section. Confirming this now allows us to fully explain the volume dependence of the complex, as shown in Table III. The volume is reduced monotonically from $Q=+2$ to $Q=-6$. For $Q=-4\rightarrow-6$ this is due simply to the change from *DX* to non-*DX*: as the Zn $4p_z$ orbital fills up, the sp^2 bonding to the P atoms is reorganized, with a normal sp^3 dangling bond developing. This can then bond on a more or less equal footing with the In dangling bonds. Then from $Q=+2\rightarrow-4$ the In-In distances are reduced as electrons enter the In dangling bonds, increasing the bonding between them. The volume reduction, however, is due only partly to this: partly it is due to the concurrent reduction in Zn-In

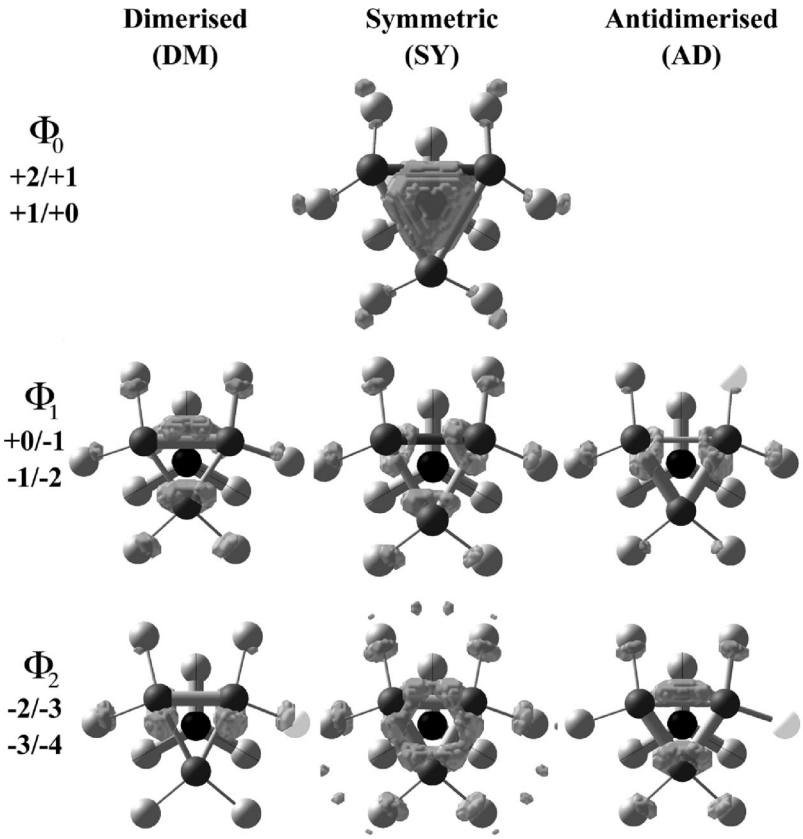

FIG. 5. Top views [down the (111) axis] of the 50% isosurface plots for charge density differences corresponding to the transfer levels of [Zn_{In}-V_P] from $Q=+2$ to -4, for the symmetric, dimerized, and antidimerized structures.

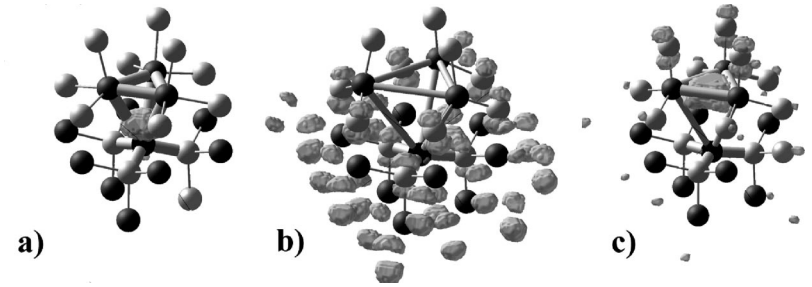

FIG. 6. Side views of charge density difference plots for (a) the Zn $4p_z$ related orbital Φ_3 filled at the $-4/-5$ and $-5/-6$ transfer levels, (b) the delocalized orbital emptied in removing an electron from $Q=+5$, and (c) the orbital emptied in removing an electron from the metastable shrunken structure for $Q=+2$.

distances, even though no bonds form between the Zn and In until $Q=-5$. This reduction is electrostatic in origin. The empty Zn $4p_z$ orbital, together with the relatively high ionicity of the Zn-P bonds (see Fig. 2), leaves the positive Zn core slightly less well screened along the direction pointing towards the three In atoms. The negative charge on the In atoms, meanwhile, increases as electrons are added, so the Zn-In distance is reduced electrostatically. Thus the reduction in effective vacancy volume at the $0/-1$ transfer level, observed in the positron annihilation studies of Slotte *et al.*,[2] is due to a combination of the In-In bonding and Zn-In electrostatic attraction, rather than to a *DX* to non-*DX* transition as might perhaps have been expected.

Regarding the other structures in Tables III and IV, we find that, as anticipated from the structures themselves, the orbitals filled by adding further electrons to $[\mathrm{Zn_{In}}\text{-}\mathrm{V_P}]^{-6}$ or removing further electrons from $[\mathrm{Zn_{In}}\text{-}\mathrm{V_P}]^{+2}$ are all delocalized. We show only one example in Fig. 6: namely, removing an electron from $+5$. The orbital emptied by removing an electron from the metastable shrunken structure of $Q=+2$ (also in Fig. 6) is identical to that associated with removing an electron from the ground structure of $Q=0$. This confirms the explanation given above of these shrunken structures in terms of holes excited off into delocalized valence-band states.

V. STRUCTURAL MODEL FOR THE $[\mathrm{Zn_{In}}\text{-}\mathrm{V_P}]$ COMPLEX

A. Symmetry considerations

Since, for $Q>-5$, the Zn is in a *DX*-like position and the Zn $4p_z$ is much higher in energy than the other orbitals involved, we omit it and base our model on the assumption that all additional electrons added (removed) from the complex go to (come from) the triangle of sp^3 hybrid dangling bonds on the In atoms. These start out life transforming as the 0^+ (s) and 1^- (p) irreducible representations of the O_3 group for the free atoms, which descend to the (one-dimensional) A_1 and (three-dimensional) T_2 representations of the tetragonal group T_d when placed inside a zinc blende structured crystal. (See the level splitting diagram in Fig. 7.) The point group of a free vacancy (without the Zn) is the same (T_d) and so the bound states inside the vacancy are known to also be described[17] by the same A_1 and T_2 representations of T_d, giving a deep symmetric level and a threefold-degenerate excited level. (Jahn-Teller distortions lifting this degeneracy lead to the negative U effects for the free $\mathrm{V_P}$.) In $[\mathrm{Zn_{In}}\text{-}\mathrm{V_P}]$ the Zn further lowers the point group to C_{3v}. The A_1 representation of T_d is projected onto the A_1 representation of C_{3v}, while the T_2 representation splits, giving a second A_1 representation and a two-dimensional E representation. The two A_1 representations can mix, so that the hybridization on the Zn is reorganized, to give the high (unoccupied) Zn $4p_z$ orbital observed in our calculations, plus a new totally symmetric level constructed primarily from the three remaining In dangling bonds. The E representation corresponds to a twofold-degenerate excited state, also constructed primarily from In dangling bonds. In the neutral state the lowest A_1 level is full and the others are empty. For charge states $Q=-1\rightarrow-3$ this degeneracy must also be lifted, usually by a further structural Jahn-Teller effect. This can happen in two ways: via the formation of one stronger or one weaker bond, leading to the C_{1v} point group, or via a process reducing the symmetry to C_3, splitting the E level into $l=\pm1$ components. The latter requires a rigid rotation of the In triangle around the (111) axis, alternately shortening and lengthening the In-P bonds in the plane perpendicular to (111). This is not likely to be favored, however, since the energy gained would be very small. Indeed, we do not see any tendency towards this in our *ab initio* structures.

For certain Q it is also possible for the degeneracies to be lifted by spin interactions. In the $Q=-1$ state, where the In triangle contains three electrons, it would be possible to localize one electron on each In—making the lower A_1 and E representations degenerate—and then form an $S=\frac{3}{2}$ high-spin state. This would require[18] the In sp^3 dangling bonds to be spatially rather small (localized) and hence local Coulomb interactions to be rather strong. This does not appear to be the case, however. In additional calculations using the local spin density approximation (LSDA) to search for it we find no evidence of such a state being stable. Similarly, in $Q=-2$, with four electrons present, an $S=1$ high-spin state could be formed in the half-filled T_2. Again, we find no indications that this is stable.

Instead, it seems that the symmetric structures for $Q=-1\rightarrow-3$ are stabilized by weak Coulomb interactions with no localization (beyond that to the In triangle itself.) We

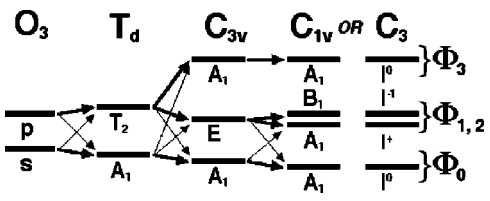

FIG. 7. Irreducible representation splittings as symmetry is lifted from O_3 to C_{1v} or C_3. For C_{1v} the dimer case is shown. For the antidimer the B_1 level lies below the second A_1 level.

can estimate the differences between the classical spatial overlaps of the three orbitals. Specifically, we take the charge contained in the overlap regions of the isocharge surfaces for charge density differences (as plotted in Figs. 3–6) renormalized to a whole electron to allow comparisons and evaluate what fraction of the charge overlaps classically. Using the 50% isocharge surfaces in Fig. 5, we find that the highest of these orbitals, Φ_2 (corresponding to transfer levels $-2/-3$ and $-3/-4$), has 58% more overlap with the lowest (Φ_0, transfer levels $+2/+1$ and $+1/0$) than the middle orbital (Φ_1, $0/-1$ and $-1/-2$) has with the lowest. (The overlap between the middle and highest is about 29 times larger again.) Using the 20% isocharge surface, where more of the actual charge is accounted for, but where the spurious defect level dispersion is starting to wash out the effect, we find that the lowest orbital has 62% more overlap with the highest than it has with the middle one. These numbers indicate that in the symmetric geometries the E level is split into orbitals having less and more overlap with the deep A_1 level. These levels are thus split by Coulomb repulsion from the electrons filling the deep A_1 level.

B. Tight-binding model

The Jahn-Teller behavior found in the *ab initio* studies can be explained using a simple tight-binding model. To do this we need only consider the leading-order effects of changes in the In-In distances. We make no assumptions yet about the form of the degenerate associated orbitals ϕ_i, and we consider only the ''hopping'' overlap matrix elements t_{ij} which move electrons between the orbitals on In_i and In_j. The Hamiltonian is simply

$$\hat{H}=\sum_{i,j;\sigma} -t_{i,j}c^{\dagger}_{j,\sigma}c_{i,\sigma}, \tag{7}$$

where $c^{\dagger}_{i,\sigma}$ ($c_{i,\sigma}$) creates (annihilates) a spin σ electron at i, the sums being over the three In atoms. We make the selection $t_{23}=t+\delta$ and $t_{12}=t-\delta/2=t_{13}$. Hence $\delta>0$ corresponds to forming a single In_2-In_3 dimer (plus two antidimers) and $\delta<0$ to a single In_2-In_3 antidimer (plus two dimers). (The $-\delta/2$ terms balancing the $+\delta$ allow direct comparisons between $\delta>0$, $=0$, and <0.) We omit Coulomb repulsion (we assume that $U\ll t$) and also the spin-spin interactions which would lead to high-spin states. On the other hand, we will treat the symmetric structures as (potentially) metastable, thus implicitly assuming the presence of (at least) a vanishing Coulomb repulsion between the E levels and the deep A_1 level. More importantly, we also omit elastic effects from the lattice. To leading order, δ is linear in the change in In-In distance, but the elastic energy is quadratic. We can therefore write the elastic energy for an individual bond between In_i and In_j as $\lambda\delta_{ij}^2 t$, where λ is (related to) an elastic constant. Hence for both the dimer and antidimer states described above the elastic energy is $\approx\lambda\delta^2 t + 2\lambda(\delta/2)^2 t=3\lambda\delta^2 t/2$. However, we omit this term at present, solving only Eq. (7).

In the dimer case ($\delta>0$) the solution is

$$E_0=-\frac{1}{2}-\frac{\delta}{2}-\frac{F(\delta)}{2}\approx-2-\frac{\delta^2}{6},$$

$$E_1=-\frac{1}{2}-\frac{\delta}{2}+\frac{F(\delta)}{2}\approx 1-\delta+\frac{\delta^2}{6}, \tag{8}$$

$$E_2=1+\delta,$$

in units of t [expansions to $O(\delta^2)$ only], where

$$F(\delta)=\sqrt{3}\sqrt{3-2\delta+\delta^2}\approx 3-\delta+\frac{\delta^2}{3}. \tag{9}$$

We write the wave functions in the form $\Phi=(a_1,a_2,a_3)$ where $\{a_i\}$ are the coefficients of $\{\phi_i\}$ in Φ. The wave functions associated with E_0, E_1, and E_2 are thus

$$\Phi_0=\left(\frac{1+\delta-F(\delta)}{\delta-2},1,1\right)\approx\left(1-\frac{\delta}{2}-\frac{\delta^2}{12},1,1\right),$$

$$\Phi_1=\left(\frac{1+\delta+F(\delta)}{\delta-2},1,1\right)\approx\left(-2-\delta-\frac{2\delta^2}{3},1,1\right), \tag{10}$$

$$\Phi_2=(0,1,-1),$$

respectively. (Normalization is omitted for clarity.) Hence, the ground state E_0 is totally bonding (an A_1 irreducible representation of C_{1v}), but has more weight upon the dimerized In_2-In_3 bond, thus corresponding to a dimer bonded to the single-site In_1. This is a very different result to that obtained[6,7,15] for the free V_P, where the lowest-lying state was totally symmetric with equal weight on all sites. This new result for [Zn_{In}-V_P] indicates that a dimer (or antidimer) may form even with only one electron present and no degeneracy. (The Jahn-Teller theorem does *not* state that symmetry *cannot* be reduced in the absence of degeneracy.) This possible symmetry lowering is weak, however: the energy gained is only $\sim\delta^2$, the same order as the elastic energy lost. It comes about because the dimerization or antidimerization breaks the E irreducible representation of C_{3v} up into a B_1 and a further A_1 representation of C_{1v}. This new A_1 representation can mix with the other ones, leading to a weak gain in energy, even though the Jahn-Teller theorem does not actually require it here. Taking elastic energy into account, the total energy of the dimer structure for $Q=+1$ (with one electron) is

$$E^{Q=+1}=-\frac{t}{2}[1+\delta+F(\delta)-3\lambda\delta^2]. \tag{11}$$

Taking the derivative of $E^{Q=+1}$ with respect to δ we find that the lowest-energy solution has $\delta>0$ (is dimerized) as long as $0<\lambda<0.17$. This appears to correspond to a weak value of the elastic constant. For $Q=-1\rightarrow-3$ a stable dimer state exists for any value of λ and has a lower energy than the symmetric structure. Our DFT calculations indicate that the case of [Zn_{In}-V_P] in InP is near to this critical value of $\lambda=0.17$: if we do the relaxation using a $4\times4\times4$ **k**-point grid, we do not find a stable dimer or a stable antidimer. However, if we use the less accurate $2\times2\times2$ **k**-point grid,

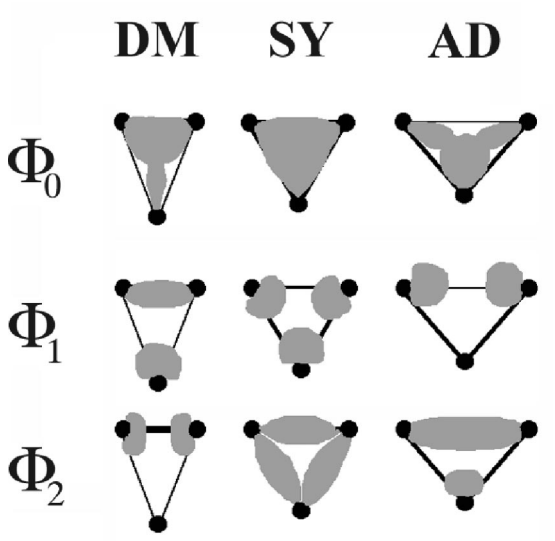

FIG. 8. Sketch of the wave functions anticipated for the three structures of $[Zn_{In}\text{-}V_P]$, based upon the model (DM=dimerized, SY=symmetric, AD=antidimerized).

we do indeed find a nonsymmetric structural ground state for $Q=+1$—namely, a 2.1%-dimerized structure, with the symmetric structure an excitation 0.002 eV above. For $Q=0$ we never find stable dimerized or antidimerized structures.

Turning to the model excitations for the dimer structure, E_1 also corresponds to an In_2-In_3 dimer (another A_1 representation), but now antibonded to the single site, upon which most of the weight is placed. E_2 is an antibonded dimer (an antidimer—a B_1 irreducible representation of C_{1v}) with no weight at all on the single site. For the antidimer structure ($\delta<0$) the ground state remains the same (at least for small δ) but there is less weight on the dimer bond and more on the single site. Also, the order of the excitations is reversed, with the antidimer state (E_3 above) becoming the lower of the two. If we now assume a form for ϕ_i related to sp^3 hybrids, we can see what sort of charge densities we expect to see for the Φ_j, as sketched in Fig. 8.

In the case of the excitations for the symmetric structure, we find

$$\Phi_{1,2}=\Phi_{\pm}=(1,e^{\pm 2\pi i/3},e^{\pm 4\pi i/3}), \tag{12}$$

with the two being, of course, degenerate. Unfortunately, describing the lifting of this degeneracy as a result of Coulomb and elastic effects (the two will almost certainly combine) lies well outside the scope of this model or paper. Hence what is shown in the figure is just the two alternatives with C_3 symmetry and three nodelike planes, based upon the form of $\Phi_{\pm}$. The one with low charge density along the In-In lines is likely to have a smaller overlap with—and hence Coulomb repulsion from—the symmetric E_0 ground state. Hence it has been drawn as the lower of the two excitations. This cannot be predicted with more certainty upon the basis of the current model calculation, however.

With the obvious exception of the excitations for the symmetric structure, the similarity between the model charge densities in Fig. 8 and the *ab initio* charge densities in Fig. 5 is clear. We are indeed seeing the predicted combinations of one-electron orbitals from the three In dangling bonds, controlled by Jahn-Teller effects which the model can also predict.

TABLE VI. Model predictions for the lowest-lying structures (marked L.L.) of $[Zn_{In}\text{-}V_P]^Q$, together with structural excitation energies to leading order in δ, for occupancies of from zero to six electrons (No. e^-). DM=dimerized, SY=symmetric, and AD=antidimerized.

No. e^-	Q	DM	SY	AD
0	+2	-	L.L.	-
1	+1	L.L.	$\frac{\delta^2 t}{6}$	$\frac{\delta^3 t}{9}$
2	0	L.L.	$\frac{\delta^2 t}{3}$	$\frac{2\delta^3 t}{9}$
3	−1	$\frac{\delta^2 t}{6}$	δt	L.L.
4	−2	$\frac{\delta^2 t}{3}$	$2\delta t$	L.L.
5	−3	$\frac{\delta^2 t}{6}$	δt	L.L.
6	−4	-	L.L.	-

Using Eq. (9) we can now evaluate the energy of the symmetric, dimerized, and antidimerized states for each value of electron filling and compare them. For example, with five electrons present ($[Zn_{In}\text{-}V_P]^{-3}$) the symmetric state has energy $-t$, the dimerized state has energy $-t(1+\delta)$, and the antidimerized state has energy $(-t/2)[1+\delta+F(\delta)]\approx -t(1+\delta+\delta^2/6)$. Hence the lowest is the antidimer, with the dimer as an excitation only $\sim\delta^2 t/6$ higher, and the symmetric state lies $\sim\delta t$ higher still. Comparing to Table V we indeed see that the antidimer is the most stable, followed by the dimer, with the symmetric structure the least stable. Table VI shows the leading terms in these excitation energies for fillings of from zero to six electrons. Since both elastic and Coulomb energies favor the symmetric structure, we anticipate only the symmetric structure for $Q=+2$ and -4, as observed. We also anticipate that the excitation energies for the symmetric forms will be lower than those indicated in the table. We find that for one or two electrons the dimerized structure is the most stable, closely followed by the antidimerized structure. For three, four, or five electrons we expect the antidimerized structure to be the lowest, with the symmetric structure always the least stable. The agreement with the *ab initio* results is very close—the only real exception is that for $Q=-3$ our *ab initio* calculations found the dimerized state to be slightly more stable than the antidimerized. The *ab initio* energy difference was tiny, however, over an order of magnitude less than the accuracy anticipated from such a calculation. On the other hand, the model does predict that the symmetric structure is at its least stable for charge $Q=-2$ and this is indeed the only charge state for which we are unable to find the symmetric structure using DFT.

VI. CONCLUSIONS

We have calculated the structure and transfer levels of the $[Zn_{In}\text{-}V_P]$ complex using *ab initio* DFT methods and have presented detailed results for the dependence of the structure and structural excitations upon the charge state of the complex and hence upon the Fermi level. We found that, for all charge states below -5, the Zn atom lies in a *DX* position, sp^2 hybridized, with an empty $4p_z$ orbital directed towards the In triangle and very constant bond lengths to the surrounding P atoms. Electrons added (below $Q=-5$) go into localized orbitals built from the three In dangling bonds—thus reducing the In-In distances with each added electron. We also found that there is a simultaneous reduction in the Zn-In distances, which is electrostatic in origin. This was due to the increased charge on the In triangle and the weaker screening of the Zn core along (111) owing to the empty Zn $4p_z$ orbital. The combination of these effects leads to a systematic reduction in the effective vacancy volume of the complex for charge states from $Q=+2\rightarrow-4$. This is in spite of the fact that the *DX* structure of the complex remains stable with rising Fermi level right up until a $-4/-6$ negative-*U* transfer level, about 0.5 eV into the conduction band. For charge states $Q=-1\rightarrow-3$ we also found complex Jahn-Teller behavior, with up to three different stable structures—symmetric, dimerized, and antidimerized—which are all very close to degeneracy. For $Q=-1$ the most stable structure (just) is dimerized, while it is antidimerized for $Q=-2$ and -3.

In addition, we have presented a simple tight-binding model which is able to predict and explain all of the structural properties of the complex, including the existence of three possible nearly degenerate structures for $Q=-1\rightarrow-3$. Such a near degeneracy between dimer and antidimer structures has not been seen for the free V_P and this too the model can predict: the same model applied to V_P^{-1}, for example, shows a separation between dimerized and antidimerized structures on the order of δ, compared to δ^2 here for $[Zn_{In}\text{-}V_P]$. (Details of these calculations will be presented elsewhere.[15]) Success with such a simple model is very pleasing and may in the future even help to narrow the range of initial configurations required when searching for structural minima in similar *ab initio* calculations.

Comparing our results to those obtained from positron annihilation experiments, we, as they, find that the most stable charge state of the $[Zn_{In}\text{-}V_P]$ complex is $Q=0$ in *p*-type material. We find a binding energy of 0.39 eV which is also in the range anticipated. Regarding the structure of the complex, we find a larger effective vacancy volume than that of the free V_P and upon excitation to the -1 charge state we see a reduction in volume of about 14%. Hence we are in agreement with the conclusions[2] of Slotte *et al.* rather than those[1] of Mahony *et al.* regarding the sign of the volume change at the $0/-1$ transfer level. Regarding the positron lifetimes themselves, the link between them and our calculated tetrahedron volumes is not direct, but our 14% volume change appears in good agreement with the 15%–20% reduction in measured positron lifetimes between the two structures, even though our calculated volume for the free vacancy itself is slightly smaller again. At 0.50 eV our position for the transfer level within the gap is a little high, but as was noted, these transfer levels are not reliable since the supercell is too small. Further studies of the complex in larger cells are required to check how this affects the position of the transfer levels, but our results seem otherwise to be in very good agreement with the experiments.

Regarding the issue of compensation, our results confirm that, should free V_P somehow be present in heavily Zn-doped InP, they would indeed form stable complexes with Zn. However, the formation energy we find for V_P is 1.96 eV, which is still rather large. Even for a phosphorus atom neighboring a Zn dopant the effective formation energy is $1.96-0.39=1.57$ eV, which is not small. The positron annihilation experiments clearly demonstrate that at least some V_P are present in heavily Zn-doped Czochralski-grown InP. However, the lack of a low formation energy leaves it unclear whether, and perhaps unlikely that, V_P generation is the primary cause of compensation in InP:Zn. On the other hand, our DFT results indicate that the formation of $[Zn_{In}\text{-}V_P]$ complexes from existing Zn_{In} and V_P is certainly *not* responsible for compensation: starting with fully ionized Zn, the complex forming reaction is

$$Zn_{In}^{-1}+V_P^{+1}\Leftrightarrow[Zn_{In}-V_P]^0, \tag{13}$$

in which no free electrons or holes are created or absorbed. The compensation issue here has to do with the formation of the phosphorus vacancies in the first place and is not affected by the subsequent formation of the $[Zn_{In}\text{-}V_P]$ complex. Fully understanding the issue of carrier compensation in InP:Zn from an *ab initio* point of view may thus require more work.

*Present address: Material Physics, Kungliga Techniska Högskolan, 229 KTH-Electrum, 16440 Kista. Electronic address: Christopher.Castleton@fysik.uu.se

[1] J. Mahony, P. Mascher, and W. Puff, J. Appl. Phys. **80**, 2712 (1996).
[2] J. Slotte, K. Saarinen, A. Salmi, S. Simula, R. Aavikko, and P. Hautojarvi, Phys. Rev. B **67**, 115209 (2003).
[3] K. Saarinen (private communication).
[4] M. Alatalo, H. Kauppinen, K. Saarinen, M. Puska, J. Mkinen, P. Hautojarvi, and R. Nieminen, Phys. Rev. B **51**, 4176 (1995).
[5] R. Jansen, Phys. Rev. B **41**, 7666 (1990).
[6] M. Alatalo, R. Nieminen, M. Puska, A.P. Seitsonen, and R. Virkkunen, Phys. Rev. B **47**, 6381 (1993).
[7] A.P. Seitsonen, R. Virkkunen, M. Puska, and R. Nieminen, Phys. Rev. B **49**, 5253 (1994).
[8] W. Kohn and L. Sham, Phys. Rev. **140**, A1133 (1965).
[9] D. Vanderbilt, Phys. Rev. B **41**, 7892 (1990).
[10] G. Kresse and J. Hafner, J. Phys.: Condens. Matter **6**, 8245 (1994).
[11] G. Kresse and J. Furthmuller, Comput. Mater. Sci. **6**, 15 (1996).
[12] Adapted from S.B. Zhang and J. Northrup, Phys. Rev. Lett. **67**, 2339 (1991).
[13] H. Monkhorst and J. Pack, Phys. Rev. B **13**, 5188 (1976).
[14] B. Silvi and A. Savin, Nature (London) **371**, 683 (1994).

[15] C. Castleton and S. Mirbt (unpublished).
[16] C. Castleton (unpublished).
[17] M. Lannoo, Physica B **116**, 63 (1982).
[18] A. Zywietz, J. Furthmuller, and F. Bechstedt, Phys. Rev. B **59**, 15 166 (1999).
[19] Alatalo *et al.* (Refs. 2 and 4) have used DFT-LDA and DFT generalized gradient approximation (GGA) calculations to estimate the positron annihilation at Zn-V_P complexes, but they included only empirical breathing mode relaxations (to fit the positron lifetimes) and presented no results for the structure, transfer levels, or energetics of the complex.
[20] Bulk values are calculated using the same pseudopotentials as we use for the defect calculations, but they are each fully converged in terms of both **k**-point grid and planewave cutoff.
[21] Certain additional structures—a dimerized structure for $[Zn_{In}\text{-}V_P]^{+1}$, dimerized and antidimerized structures for $[Zn_{In}\text{-}V_P]^{-4}$, and a second weaker dimer structure for $[Zn_{In}\text{-}V_P]^{-2}$—are found when the $2\times2\times2$ Monkhorst-Pack **k**-point grid is used. However, these turn out to be unstable when recalculated using a $4\times4\times4$ **k**-point grid.